Proceedings of ICAR 2003
The 11th International Conference on Advanced Robotics
Coimbra, Portugal, June 30 - July 3, 2003

# Position and Force Control of a Walking Hexapod

**Manuel F. Silva  J. A. Tenreiro Machado**

Department of Electrical Engineering
Institute of Engineering of Porto
Rua Dr. António Bernardino de Almeida, 4200-072 Porto, Portugal
Email: {mfsilva,jtm}@dee.isep.ipp.pt

## Abstract

*This paper compares the performance of classical position PD algorithm with a cascade controller involving position and force feedback loops, for multi-legged locomotion systems and variable ground characteristics. For that objective the robot prescribed motion is characterized in terms of several locomotion variables. Moreover, we formulate several performance measures of the walking robot based on the robot and terrain dynamical properties and on the robot hip and foot trajectory errors. Several experiments reveal the performance of the different control architectures in the proposed indices.*

## 1. Introduction

Walking machines allow locomotion in terrain inaccessible to other type of vehicles, since they do not need a continuous support surface [3]. On the other hand, the requirements for leg coordination and control impose difficulties beyond those encountered in wheeled robots [6]. There exists a class of walking machines for which walking is a natural dynamic mode. Once started on a shallow slope, a machine of this class will settle into a steady gait, without active control or energy input [4]. However, the capabilities of these machines are quite limited. Previous studies focused mainly in the control at the leg level and leg coordination using neural networks [10], fuzzy logic [9], hybrid force/position control [5] and subsumption architecture [1]. There is also a growing interest in using insect locomotion schemes to control walking robots at the leg level and leg coordination [2]. Nevertheless, the control at the joint level is almost always implemented using a simple *PID* like scheme with position/velocity feedback.

The present study compares two different robot control architectures, namely a Proportional-Derivative position algorithm (*PD-P*) and a cascade of a Proportional-Derivative position control with foot force feedback (*PD-P&F*). The aim is to verify the performance of the two control architectures and the influence of foot force feedback on the system stability and robustness for variable ground characteristics.

The analysis is based on the formulation of several indices measuring the robot and ground dynamics as well as the hip and foot trajectory errors during walking.

Several simulations reveal the superior performance of the control architecture with foot force feedback that minimizes the proposed indices, particularly in real situations where we have non-ideal actuators with saturation.

Bearing these facts in mind, the paper is organized as follows. Section two introduces the hexapod model and the motion planning scheme. Sections three and four present the robot control architecture and formulate the optimizing indices, respectively. Section five develops a set of experiments that reveal the performance of the different control architectures. Finally, section six outlines the main conclusions and directions towards future developments.

## 2. A Model for Multi-Legged Locomotion

We consider a walking system with $n$ legs, equally distributed along both sides of the robot body, having each one two rotational joints (Fig. 1).

Motion is described by means of a world coordinate system. The kinematic model comprises: the cycle time $T$, the duty factor $\beta$, the transference time $t_T = (1-\beta)T$, the support time $t_S = \beta T$, the step length $L_S$, the stroke pitch $S_P$, the body height $H_B$, the maximum foot clearance $F_C$, the $i^{th}$ leg lengths $L_{i1}$ and $L_{i2}$ and the foot trajectory offset $O_i$ ($i$=1,…,$n$). Moreover, we consider a periodic trajectory for each foot, with body velocity $V_F = L_S / T$.

Given a particular gait and duty factor $\beta$, it is possible to calculate for leg $i$ the corresponding phase $\phi_i$ and the time instant where each leg leaves and returns to contact with the ground [6].

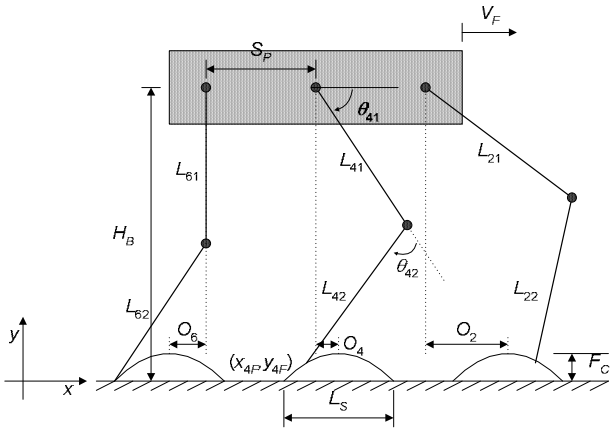


Fig. 1. Coordinate system and variables that characterize the motion trajectories of the multi-legged robot

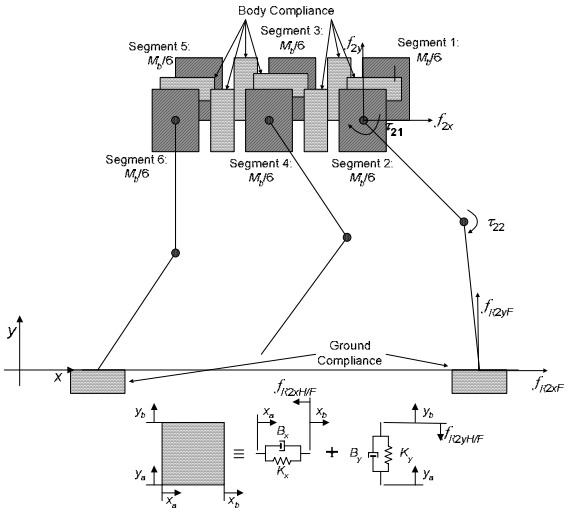


Fig. 2. Model of the robot body and foot-ground interaction

From these results, and knowing $T$, $\beta$ and $t_S$, the cartesian trajectories of the tip of the foots must be completed during $t_T$. Based on this data, the trajectory generator is responsible for producing a motion that synchronises and coordinates the legs.

For each cycle the desired trajectory of the tip of the swing leg is computed through a cycloid function given by (considering, for example, that the transfer phase starts at $t = 0$ s for leg 1), with $f = 1/T$:

- during the transfer phase:

$$x_{1Fd}(t) = V_F\left[t - \frac{1}{2\pi f}\sin(2\pi ft)\right] \quad (1a)$$

$$y_{1Fd}(t) = \frac{F_C}{2}\left[1 - \cos(2\pi ft)\right] \quad (1b)$$

- during the stance phase:

$$x_{1Fd}(t) = V_F T \quad (2a)$$

$$y_{1Fd}(t) = 0 \quad (2b)$$

The body of the robot, and by consequence the legs hips, is assumed to have a desired horizontal movement with a constant forward speed $V_F$. Therefore, for leg $i$ the cartesian coordinates of the hip of the legs are given by:

$$\mathbf{p_{Hd}}(t) = \begin{bmatrix} x_{iHd}(t) \\ y_{iHd}(t) \end{bmatrix} = \begin{bmatrix} V_F t \\ H_B \end{bmatrix} \quad (3)$$

From the coordinates of the hips and feet of the robot it is possible to obtain the leg joint positions and velocities using the inverse kinematics $\boldsymbol{\psi}^{-1}$ and the Jacobian $\mathbf{J} = \partial\boldsymbol{\psi}/\partial\boldsymbol{\theta}$.

The algorithm for the forward motion planning accepts the desired cartesian trajectories of the leg hips $\mathbf{p_{Hd}}(t) = [x_{iHd}(t), y_{iHd}(t)]^T$ and feet $\mathbf{p_{Fd}}(t) = [x_{iFd}(t), y_{iFd}(t)]^T$ as inputs and, by means of an inverse kinematics algorithm, generates the related joint trajectories $\boldsymbol{\theta_d}(t) = [\theta_{i1d}(t), \theta_{i2d}(t)]^T$, selecting the solution corresponding to a forward knee:

$$\mathbf{p_d}(t) = \begin{bmatrix} x_{id}(t) \\ y_{id}(t) \end{bmatrix} = \mathbf{p_{Hd}}(t) - \mathbf{p_{Fd}}(t) \quad (4a)$$

$$\mathbf{p_d}(t) = \boldsymbol{\psi}\left[\boldsymbol{\theta_d}(t)\right] \Rightarrow \boldsymbol{\theta_d}(t) = \boldsymbol{\psi}^{-1}\left[\mathbf{p_d}(t)\right] \quad (4b)$$

$$\dot{\boldsymbol{\theta}}_\mathbf{d}(t) = \mathbf{J}^{-1}\left[\dot{\mathbf{p}}_\mathbf{d}(t)\right] \quad (4c)$$

In order to avoid the impact and friction effects, at the planning phase we estimate null velocities of the feet in the instants of landing and taking off, assuring also the velocity continuity.

Figure 2 presents the model for the hexapod body and foot-ground interaction.

The contact of the $i^{th}$ robot feet with the ground is modeled through a linear system with damping $B_{ix}$ ($B_{iy}$) and stiffness $K_{ix}$ ($K_{iy}$) in the horizontal (vertical) directions, respectively.

The same type of model is adopted to implement the compliance between the $n$ segments of the robot body. Therefore, we divide the robot body in $n$ identical segments, each segment (with mass $M_b/n$) corresponding to a robot hip connected to the neighbor segments through a spring-dashpot model.

## 3. Hexapod Robot Control Architecture

The planned joint trajectories constitute the reference for the robot control system. The model for the robot inverse dynamics is formulated as:

$$\boldsymbol{\tau} = \mathbf{H}(\boldsymbol{\theta})\ddot{\boldsymbol{\theta}} + \mathbf{c}\left(\boldsymbol{\theta}, \dot{\boldsymbol{\theta}}\right) + \mathbf{g}(\boldsymbol{\theta}) - \mathbf{J^T_H}(\boldsymbol{\theta})\mathbf{F_{RH}} - \mathbf{J^T_F}(\boldsymbol{\theta})\mathbf{F_{RF}} \quad (5)$$

where $\boldsymbol{\tau} = [f_{ix}, f_{iy}, \tau_{i1}, \tau_{i2}]^T$ ($i$=1,…,$n$) is the vector of forces/torques, $\boldsymbol{\theta} = [x_{iH}, y_{iH}, \theta_{i1}, \theta_{i2}]^T$ is the vector of position coordinates, $\mathbf{H}(\boldsymbol{\theta})$ is the inertia matrix and $\mathbf{c}\left(\boldsymbol{\theta}, \dot{\boldsymbol{\theta}}\right)$ and $\mathbf{g}(\boldsymbol{\theta})$ are the vectors of centrifugal/Coriolis and gravitational forces/torques, respectively. The $n \times m$ matrices $\mathbf{J^T_H}(\boldsymbol{\theta})$ and $\mathbf{J^T_F}(\boldsymbol{\theta})$ are the transposes of the robot Jacobian matrices, $\mathbf{F_{RH}}$ is the $m \times 1$ vector of the body inter-segment forces and $\mathbf{F_{RF}}$ is the $m \times 1$ vector of the reaction forces that the ground exerts on the robot feet (these forces are null during the foot transfer phase).

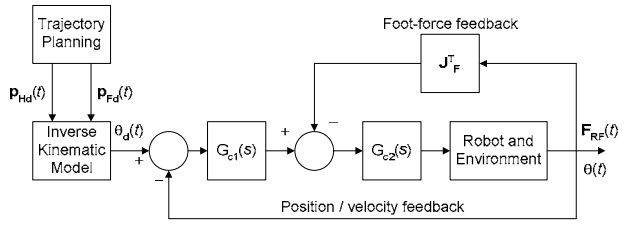


Fig. 3. Hexapod robot control architecture

Furthermore, we consider that the joint actuators are not ideal, exhibiting a torque limitation (*i.e.*, actuator saturation) given by:

$$T_{mij} = \begin{cases} T_{Cij} & , \left|T_{mij}\right| \le T_{Max} \\ \text{sgn}\left(T_{Cij}\right) \cdot T_{Max} & , \left|T_{mij}\right| > T_{Max} \end{cases} \quad (6)$$

where, for leg $i$ and joint $j$, $T_{Cij}$ is the controller demanded torque, $T_{Max}$ is the maximum torque that the actuator can supply and $T_{mij}$ is the motor effective torque.

The general control architecture of the hexapod robot is presented in Fig. 3. The joint reference trajectories are generated using (4a), (4b) and (4c). For the controller $G_{c1}(s)$ we adopt a position/velocity *PD* algorithm:

$$G_{C1j}(s) = Kp_j + Kd_j s \quad , j = 1,2 \quad (7)$$

where $Kp_j$ and $Kd_j$ are the proportional and derivative gains for joint $j$. For $G_{c2}(s)$ we consider a simple *P* controller. Furthermore, we consider two control architectures namely a simple joint position/velocity feedback (*PD-P*) and a cascade joint position/velocity and foot force feedback (*PD-P&F*).

In order to tune the controller parameters we adopt a "brute-force" method, testing and evaluating several possible combinations of controller parameters for both control architectures. Since the essence of locomotion is to move smoothly the section of the upper body from one place to another with some restrictions in terms of execution time we select, for each controller, the set of parameters (see Table I) that minimises the mean square errors of the robot hip trajectory ((11a) and (11b)) during one step.

## 4. Measures for Performance Evaluation

In mathematical terms we provide several global measures of the overall performance of the mechanism in an average sense [7], [8]. In this perspective we define three indices $\{E_{av}, T_L, F_L\}$ based on the robot dynamics and four indices $\{\varepsilon_{xH}, \varepsilon_{yH}, \varepsilon_{xF}, \varepsilon_{yF}\}$ based on the trajectory tracking errors.

A first measure in this analysis is the mean absolute energy per travelled distance. This index is computed assuming that energy regeneration is not available by actuators doing negative work, that is, by taking the absolute value of the power. At a given joint $j$ (each leg has $m = 2$ joints) and leg $i$ (since we are adopting an hexapod it yields $n = 6$ legs), the mechanical power is the product of the motor torque and angular velocity. The global index $E_{av}$ is obtained by averaging the mechanical absolute energy delivered over the travelled distance $L$:

$$E_{av} = \frac{1}{L}\sum_{i=1}^{n}\sum_{j=1}^{m}\int_0^T \left|\boldsymbol{\tau}_{ij}(t)\cdot\dot{\boldsymbol{\theta}}_{ij}(t)\right| dt \quad (8)$$

Therefore, a good performance requires the minimization $E_{av}$.

Another alternative optimisation strategy addresses the power lost in the joint actuators per travelled distance $L$. From this point of view, the index $T_L$ can be defined as:

$$T_L = \frac{1}{L}\sqrt{\sum_{i=1}^{n}\sum_{j=1}^{m}\int_0^T \left[\boldsymbol{\tau}_{ij}(t)\right]^2 dt} \quad (9)$$

The most suitable trajectory is the one that minimizes $T_L$.

A complementary measure considers the forces that occur on the hips of the robot per travelled distance $L$. The index $F_L$ is defined as:

$$F_L = \frac{1}{L}\sqrt{\sum_{i=1}^{n}\sum_{j=1}^{m}\int_0^T \left\{\left[f_{ix}(t)\right]^2 + \left[f_{iy}(t)\right]^2\right\} dt} \quad (10)$$

The best trajectory is the one that minimizes $F_L$.

In what concerns the hip and foot trajectory following we can define the indices:

$$\varepsilon_{xH(t)} = \sum_{i=1}^{n}\sqrt{\frac{1}{N_S}\sum_{k=1}^{N_S}\Delta_{ixH}{}^2}, \quad \Delta_{ixH} = x_H^d(k) - x_H^r(k) \quad (11a)$$

$$\varepsilon_{yH(t)} = \sum_{i=1}^{n}\sqrt{\frac{1}{N_S}\sum_{k=1}^{N_S}\Delta_{iyH}{}^2}, \quad \Delta_{iyH} = y_H^d(k) - y_H^r(k) \quad (11b)$$

$$\varepsilon_{xF(t)} = \sum_{i=1}^{n}\sqrt{\frac{1}{N_S}\sum_{k=1}^{N_S}\Delta_{ixF}{}^2}, \quad \Delta_{ixF} = x_F^d(k) - x_F^r(k) \quad (11c)$$

$$\varepsilon_{yF(t)} = \sum_{i=1}^{n}\sqrt{\frac{1}{N_S}\sum_{k=1}^{N_S}\Delta_{iyF}{}^2}, \quad \Delta_{iyF} = y_F^d(k) - y_F^r(k) \quad (11d)$$

where $N_S$ is the total number of samples for averaging purposes, $x^r_H$ ($x^r_F$) and $x^d_H$ ($x^d_F$) are the $i^{\text{th}}$ samples of the real and desired horizontal positions at the hip (foot)

section, respectively, while $y^r_H$ ($y^r_F$) and $y^d_H$ ($y^d_F$) are the $i^{th}$ samples of the real and desired vertical positions at the hip (foot).

## 5. Simulation Results

In this section we develop a set of simulations to compare the controller performances during a periodic wave gait. Consequently, we consider the parameters $\beta = 50\%$, $L_S = 1$ m, $H_B = 1.8$ m, $F_C = 0.2$ m, $V_F = 1$ ms$^{-1}$, $S_P = 1$ m, $L_{i1} = L_{i2} = 1$ m, $O_i = 0$ m, $M_{i1} = M_{i2} = 1$ kg, $M_b = 87.4$ kg and $M_{if} = 0$ kg. The robot body is modelled with $K_{ix} = 10^5$ Nm$^{-1}$, $K_{iy} = 10^4$ Nm$^{-1}$, $B_{ix} = 10^3$ Nsm$^{-1}$ and $B_{iy} = 10^2$ Nsm$^{-1}$. Furthermore, for the base experiment, the ground properties are characterised by $K_{ix} = 10^5$ Nm$^{-1}$, $K_{iy} = 10^6$ Nm$^{-1}$, $B_{ix} = 10^3$ Nsm$^{-1}$ and $B_{iy} = 10^4$ Nsm$^{-1}$.

As discussed previously, the controllers are tuned using a "brute-force" method assuming that the robot actuators are almost ideal (the maximum actuator torque in (6) is $T_{Max} = 400$ Nm). The minimisation of the hips and feet trajectories errors, leads to the $G_{c1}(s)$ controller parameters presented in Table I and a proportional controller $G_{c2}(s)$ with gain $Kp_j = 1.0$ or $Kp_j = 0.9$, in the *PD-P* or *PD-P&F* cases, respectively.

For this set of robot, ground and controller parameters the *PD-P&F* control architecture, improves the hip and foot trajectory tracking (Figs. 4 – 5), while minimising the corresponding joint torques (Figs. 6 – 7).

Based on this experiment we decided to test the controller performances for different ground properties. Therefore, in a first phase we start by considering the *PD-P* controller and different values of $K_{ix}$, $K_{iy}$, $B_{ix}$ and $B_{iy}$, in order to observe its influence upon the proposed indices, for $T_{Max} = 400$ Nm. In a second phase we repeat the experiments for the case of a *PD-P&F* control architecture.

The performance measures versus the percentage of variation of ground parameters with relation to base experiment %($K_{ix}$, $K_{iy}$, $B_{ix}$, $B_{iy}$) are presented in Figs. 8 – 11. We conclude that the robot hips and feet trajectories errors are smaller when we adopt a *PD-P&F* control architecture, for all range of variation.

Table I $G_{c1}(s)$ Controller Parameters

| | | | |
|---|---|---|---|
| *PD-P* | Joint $j = 1$ | $Kp_1$ | 80000 |
| | | $Kd_1$ | 250 |
| | Joint $j = 2$ | $Kp_2$ | 120000 |
| | | $Kd_2$ | 50 |
| *PD-P&F* | Joint $j = 1$ | $Kp_1$ | 20500 |
| | | $Kd_1$ | 110 |
| | Joint $j = 2$ | $Kp_2$ | 22000 |
| | | $Kd_2$ | 150 |

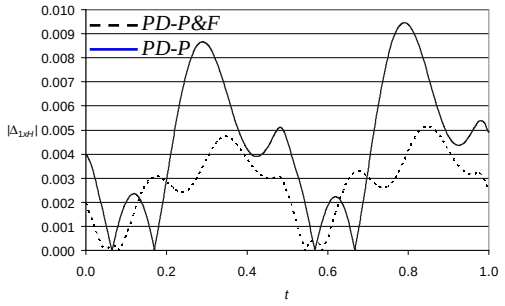


Fig. 4. Plots of the hip trajectory error $|\Delta_{1xH}|$ *vs.* $t$ for the *PD-P* and *PD-P&F* control architectures, with $T_{Max} = 400$ Nm

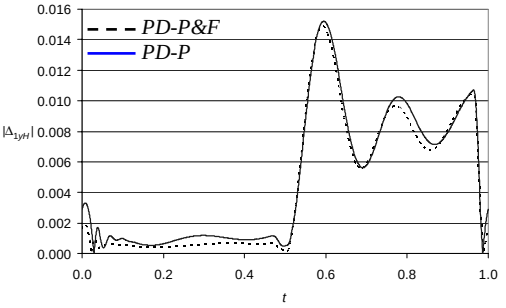


Fig. 5. Plots of the hip trajectory error $|\Delta_{1yH}|$ *vs.* $t$ for the *PD-P* and *PD-P&F* control architectures, with $T_{Max} = 400$ Nm

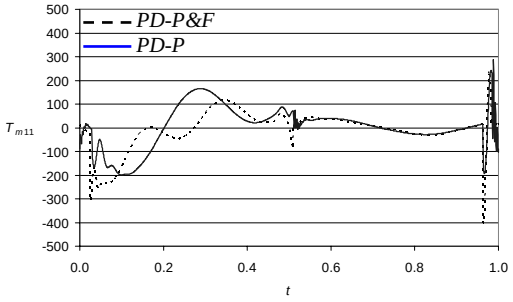


Fig. 6. Plots of the joint torque $T_{m11}$ *vs.* $t$ for the *PD-P* and *PD-P&F* control architectures, with $T_{Max} = 400$ Nm

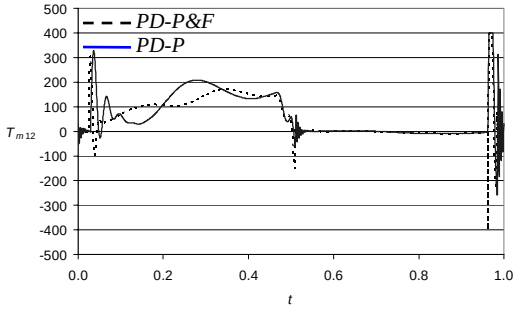


Fig. 7. Plots of the joint torque $T_{m12}$ *vs.* $t$ for the *PD-P* and *PD-P&F* control architectures, with $T_{Max} = 400$ Nm

For moderate levels of actuator saturation (*e.g.*, $T_{Max}$ = 170 Nm), Figs. 12 –15, we get similar conclusions.

In the case of strong actuator saturation (*e.g.*, $T_{Max}$ < 160 Nm) the indices reveal a large performance degradation with difficulties both for the *PD-P&F* and the *PD-P* controllers. Nevertheless, this situation is not realistic since it corresponds to operating conditions requiring joint torques much higher than those established by the saturation level. On the other hand, when we have almost ideal actuators (*e.g.*, $T_{Max}$ > 400 Nm), the *PD-P&F* scheme reveals stability problems, particularly on hard terrains (values of the ground parameters above 100% of the base values) due to the impulses of force feedback during the impacts of the feet with the ground (Figs. 16 – 17). However, this situation is also not realistic since it assumes ideal actuators exhibiting infinite joint driving torque and infinite bandwidth.

In conclusion, the foot-force feedback seems essential for a robust control performance during walking in terrain with variable dynamical characteristics.

## 6. Conclusions

In this paper we have compared the performance of *PD* control algorithms with position or position and force feedback, in hexapod robots, for variable ground characteristics. Furthermore, we evaluated how the different robot controller architectures respond to non-ideal joint actuators, namely with torque saturation, and variable ground dynamic properties.

For analyzing the system performance several quantitative measures were defined based on the robot dynamics and the hip and foot trajectory errors. The experiments reveal that the *PD-P&F* control architecture is superior to the classical *PD-P* control scheme, from the point of view of the proposed indices.

While our focus has been on a dynamic analysis in periodic gaits and actuators with saturation, many aspects of locomotion are not necessarily captured by the proposed measures. Consequently, future work in this area will address the refinement of our models to incorporate other characteristics of the robot actuators and the joint transmissions.

## References


[1] R. A. Brooks, "A Robot That Walks; Emergent Behaviours From a Carefully Evolved Network", *A.I. Memo 1091*, Artificial Intelligence Laboratory, MIT, 1989.

[2] C. Ferrell, "A Comparison of Three Insect Inspired Locomotion Controllers", *Robotics and Autonomous Systems*, **16**, pp. 135 – 159, 1995.


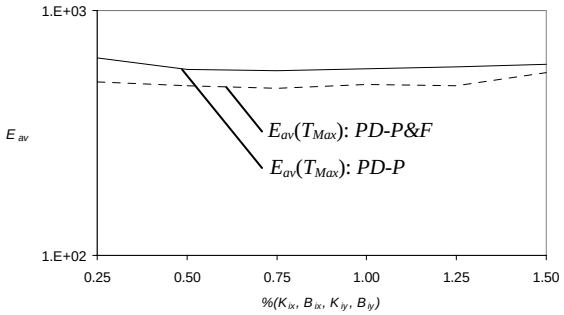


Fig. 8. Plot of $E_{av}$ *vs.* %($K_{ix}$, $K_{iy}$, $B_{ix}$, $B_{iy}$) for the *PD-P* and the *PD-P&F* control architectures, with $T_{Max}$ = 400 Nm

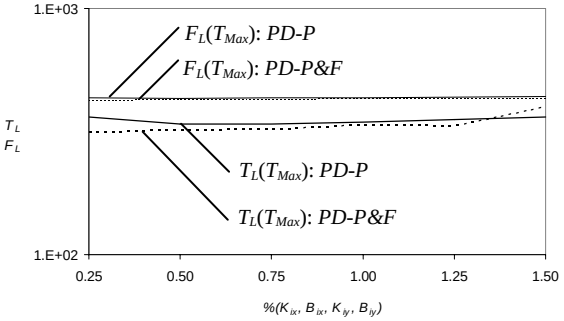


Fig. 9. Plots of $P_L$ and $T_L$ *vs.* %($K_{ix}$, $K_{iy}$, $B_{ix}$, $B_{iy}$) for the *PD-P* and the *PD-P&F* control architectures, with $T_{Max}$ = 400 Nm

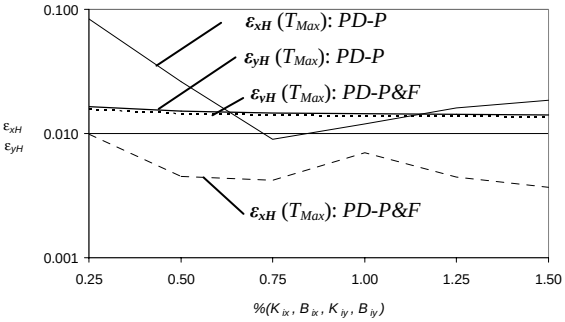


Fig. 10. Plots of $\varepsilon_{xH}$ and $\varepsilon_{yH}$ *vs.* %($K_{ix}$, $K_{iy}$, $B_{ix}$, $B_{iy}$) for the *PD-P* and the *PD-P&F* control architectures, with $T_{Max}$ = 400 Nm

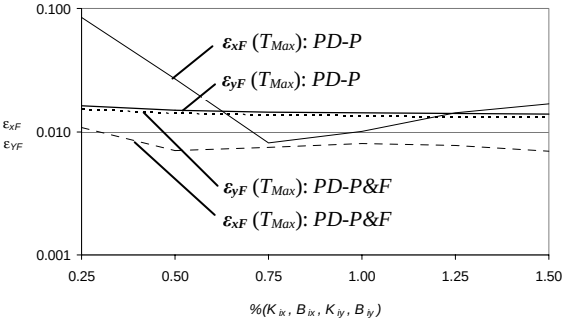


Fig. 11. Plots of $\varepsilon_{xF}$ and $\varepsilon_{yF}$ *vs.* %($K_{ix}$, $K_{iy}$, $B_{ix}$, $B_{iy}$) for the *PD-P* and the *PD-P&F* control architectures, with $T_{Max}$ = 400 Nm

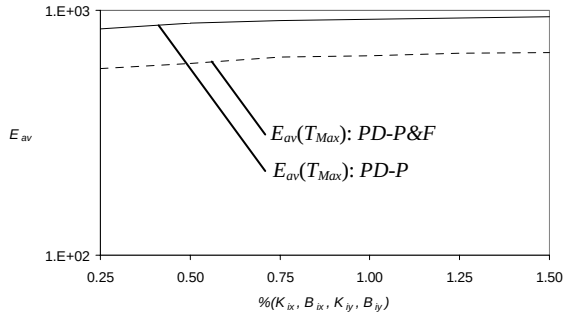


Fig. 12. Plot of $E_{av}$ *vs.* %($K_{ix}$, $K_{iy}$, $B_{ix}$, $B_{iy}$) for the *PD-P* and the *PD-P&F* control architectures, with $T_{Max}$ = 170 Nm

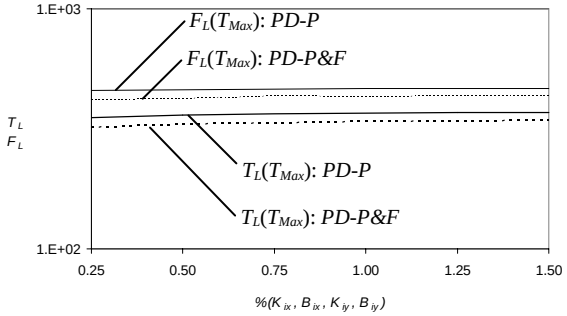


Fig. 13. Plots of $P_L$ and $T_L$ *vs.* %($K_{ix}$, $K_{iy}$, $B_{ix}$, $B_{iy}$) for the *PD-P* and the *PD-P&F* control architectures, with $T_{Max}$ = 170 Nm

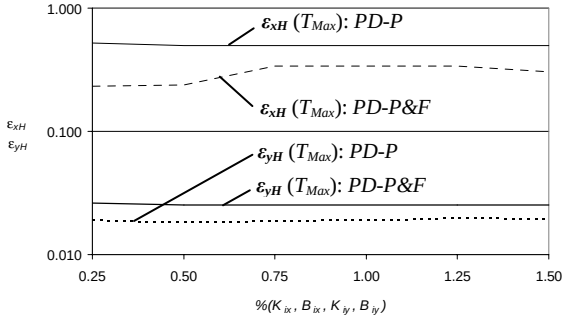


Fig. 14. Plots of $\varepsilon_{xH}$ and $\varepsilon_{yH}$ *vs.* %($K_{ix}$, $K_{iy}$, $B_{ix}$, $B_{iy}$) for the *PD-P* and the *PD-P&F* control architectures, with $T_{Max}$ = 170 Nm

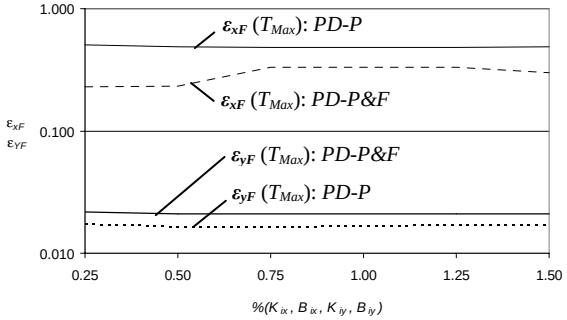


Fig. 15. Plots of $\varepsilon_{xF}$ and $\varepsilon_{yF}$ *vs.* %($K_{ix}$, $K_{iy}$, $B_{ix}$, $B_{iy}$) for the *PD-P* and the *PD-P&F* control architectures, with $T_{Max}$ = 170 Nm

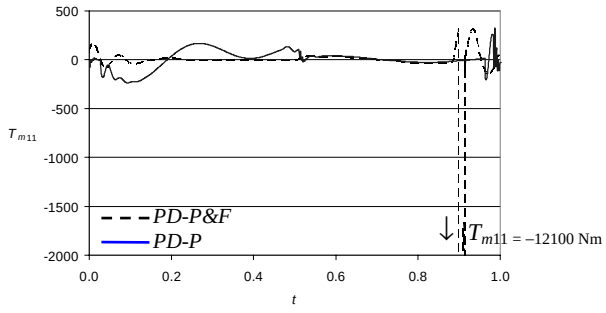


Fig. 16. Plots of the of the joint torque $T_{m11}$ *vs.* *t* for the *PD-P* and the *PD-P&F* control architectures, with $T_{Max} \rightarrow \infty$

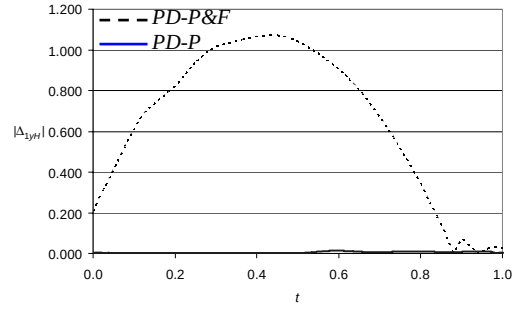


Fig. 17. Plots of the hip trajectory error $|\Delta_{1yH}|$ *vs.* *t* for the *PD-P* and the *PD-P&F* control architectures, with $T_{Max} \rightarrow \infty$


[3] D. J. A. Manko, *General Model of Legged Locomotion on Natural Terrain*, Kluwer, Westinghouse Electric Corporation, 1992.

[4] T. McGeer, "Passive Dynamic Walking", *Int. Journal of Robotics Research*, **9**, pp. 62 – 82, 1990.

[5] J. Song, K. H. Low and W. Guo, "A Simplified Hybrid Force/Position Controller Method for the Walking Robots", *Robotica*, **17**, pp. 583 – 589, 1999.

[6] S.-M. Song and K. J. Waldron, *Machines that Walk: The Adaptive Suspension Vehicle*, The MIT Press, 1989.

[7] M. F. Silva, J. A. T. Machado and A. M. Lopes, "Performance Analysis of Multi-Legged Locomotion Systems", *Proc. IEEE Int. Conf. on Robotics and Automation*, Washington, USA, pp. 2234–2239, 2002.

[8] M. F. Silva, J. A. T. Machado and A. M. Lopes, "Power Analysis of Multi-Legged Systems", *Proc. b'02 – 15th IFAC World Congress on Automatic Control*, Barcelona, Spain, 2002.

[9] C.-R. Tsai, T.-T. Lee and S.-M. Song, "Fuzzy Logic Control of a Planetary Gear Type Walking Machine Leg", *Robotica*, **15**, pp. 533 – 546, 1997.

[10] C.-R. Tsai and T.-T. Lee, "A Study of Fuzzy-Neural Force Control for a Quadrupedal Walking Machine", *Journal of Dynamic Systems, Measurement and Control*, **120**, pp. 124 – 133, 1998.